Synchronous Vibration Suppression of Magnetic Bearing Systems without Angular Sensors

Hongbo Sun, *Student Member*, *IEEE*, Dong Jiang, *Senior Member*, *IEEE*, and Jichang Yang

***Abstract*—Active Magnetic Bearing (AMB) levitates rotor by magnetic force without friction, and it can provide active control force to suppress vibration while rotating. Most of vibration suppressing methods need angular speed sensors to obtain rotating speed, but in many occasions, angular speed sensor is difficult to install or is difficult to guarantee reliability. This paper proposed a vibration suppressing strategy without angular speed sensor based on generalized integrator and frequency locked loop (GI-FLL) and phase shift generalized integrator (PSGI). GI-FLL and high-pass filter estimate frequency from control current, PSGI is applied to generate compensating signal. Firstly, model of AMB system expressed by transfer function is established and effect of centrifugal force is analyzed. Then, principle and process of vibration suppressing strategy is introduced. Influence of parameters are analyzed by root locus and bode diagram. Simulation results display the process of frequency estimation and performance of displacement. Experiments are carried on a test rig, results of simulations and experiments demonstrate the effectiveness of proposed vibration suppressing strategy.**

***Index Terms*—Active Magnetic Bearing (AMB), vibration suppression, frequency estimation, phase shift generalized integrator (PSGI)**

I. Introduction

In many occasions where required high rotating speed, such as high-speed motor and flywheel energy storage, Active Magnetic Bearing (AMB) has been used to support the rotating rotor to eliminate friction and active control. Vibration is a common problem in rotating machine, which is difficult to solve by traditional bearings. AMB can provide possibility of vibration suppression with its controllable stiffness.

As a result of processing error, the geometric center and gravity center of rotor cannot coincide, which will produce centrifugal force when rotor rotating. In AMB system, centrifugal force causes displacement of rotor off center, and the off-center signal causes current fluctuation in coil by sensor, controller and amplifier. Vibration of displacement and current are two main vibration in AMB system. Centrifugal force is main source of vibration, as a result, frequency of vibration in AMB is mainly rotating frequency.

Manuscript received August 31, 2020; revised January 18, 2021; accepted February 22, 2021. date of publication March 25, 2021; date of current version March 18, 2021.

This work was supported in part by the National Natural Science Foundation of China (NSFC) under Grant 51877091. *(Corresponding author: Dong Jiang.)*

Hongbo Sun, Dong Jiang, Jichang Yang are with the State Key Laboratory of Advanced Electromagnetic Engineering and Technology, Huazhong University of Science and Technology, Wuhan 430074, China (e-mail: hongbo_sun@hust.edu.cn ,jiangd@hust.edu.cn, yangjc@hust.edu.cn)

Digital Object Identifier 10.30941/CESTEMS.2021.00009

Suppressing vibration benefits to improve stability and accuracy of rotating, which is necessary. Vibration suppressing strategy can be mainly divided into two types, which are *auto balancing* and *vibration compensating*. Auto balancing methods mainly applies generalized notch filters to filter out synchronous component in displacement signal to reduce current fluctuation. Shiqiang Zheng[2] et al. applied coordinate transformation with low-pass filter to obtain synchronous component, and subtracted synchronous component to reduce vibration in current. It needs displacement signals of two orthogonal degrees. R. Herzog[3] et al. propose a generalized notch filter (GNF) which is inserted into the multivariable feedback without destabilizing the closed loop. Many methods of auto balancing have developed based on this method. Peiling Cui[4] applied GNFs with different resonant frequency in parallel to reduce harmonic vibration in current. Cong Peng[5] et al. applied variable phase lead in different rotating speed to stable the system by GNF. For vibration compensating, Kejian Jiang[6] et al. propose a searching strategy by parameter iterating to compensate centrifugal force. Chuan Mao[7] et al. improved this method to variable step size and searched in fewer detecting directions. Zaidong Hu[8] applied Beetle Antennae Search (BAS) Algorithm to compensate centrifugal force by iteration. Chao Bi[9] et al. presented Automatic Learning Control (ALC) based on Iterative Learning Control (ILC) and applied it to generate compensating signal to reduce vibration.

In most of vibration suppressing methods, information of rotating speed is necessary. Speed signal is usually obtained by angular sensor. But in many occasions, it is difficult to install an angular sensor, or angular sensor is damaged easily. As a result, some methods are applied to estimate rotating speed. Wook-Jin Lee[10] applied phase locked loop to estimate rotating speed and applied it to vibration suppression. Qi Chen[11] proposed a frequency estimator to obtain rotating speed. Both of these two methods have to utilize information of the rotor in two degrees of freedom, and the symmetry of these two degrees of freedom affects the result of frequency estimation. This paper proposes a strategy to reduce synchronous vibration based on phase shift generalized integration (PSGI) and frequency locked loop (GI-FLL). The information of angular speed is obtained from control current by GI-FLL and high-pass filter from one degree of freedom instead of two, then PSGI is applied to generate compensating signal to suppress vibration in displacement.

This paper is arranged as follow. In part II, transfer function from centrifugal force to displacement is analyzed, and

amplitude and phase of synchronous vibration are obtained. The analysis and process of GI-FLL and PSGI are also introduced in part II, the parameters are selected by analyzing root locus. Results of simulations are shown in part III. Experiment results carried on a test rig are shown in part IV. Simulation results and experiment results demonstrate the effectiveness of proposed vibration suppressing strategy. Conclusions are summarized in part V.

II. Vibration Suppression Strategy

In this section, model of AMB is established based on transfer function. Effect of centrifugal force is analyzed in part A and vibration suppressing strategy is introduced in part B. Method of Parameters selecting based on root locus is also introduced.

A. Model of AMB System and Unbalance Analysis

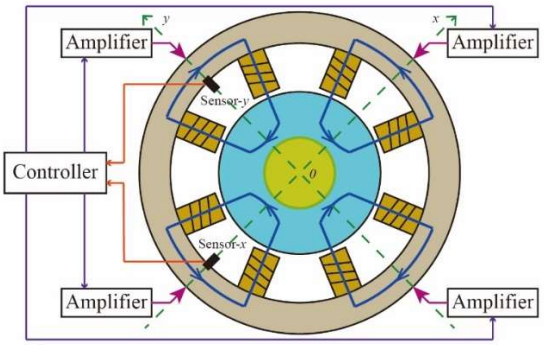

Fig. 1. Structure of radial AMB

A typical eight-pole structure radial AMB is shown in Fig. 1. Two degrees of freedom are set in orthogonal to share load average relatively. When a rotor rotating levitated by AMBs, the centrifugal force will cause synchronous vibration in radial. The displacement sensor detects position of rotor and transform it to electric signal. The controller generates instruction by information of displacement and control algorithm. The amplifier is usually chosen as current controller combined with switching converter, which produces actual current according to instruction from displacement controller. The current in coils produces magnetic force to levitate the rotor. Proportional-Integral-Differential (PID) control algorithm is widely used in displacement controller. When applying PID control and ignoring the coupling effect from other degrees of freedom, the control system can be expressed in Fig. 2.

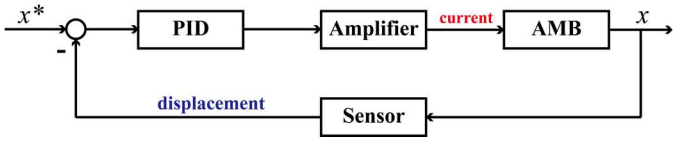

Fig. 2. Structure of PID control system

According to Newton's law, the dynamic function of rotor with magnetic force can be expressed as

$$k_i i + k_x x = m\ddot{x} \tag{1}$$

Where m is mass of rotor, k_i is force-current stiffness and k_x is force-displacement stiffness of magnetic bearing. Applying Laplace transformation, the transfer function of magnetic bearing can be obtained

$$G(s)=\frac{X(s)}{I(s)}=\frac{k_i}{ms^2-k_x} \tag{2}$$

When applying PID control strategy, the transfer function of controller can be expressed as

$$C(s)=k_p+\frac{k_I}{s}+k_D s \tag{3}$$

The amplifier has low-pass feature, transfer function of which can be expressed as

$$G_1(s)=\frac{\omega_c}{s+\omega_c} \tag{4}$$

The sensor is regarded as a linear, whose gain is k_h. Unbalance mass equivalent to the centrifugal force operating on the rotor. When the centrifugal force operates on the rotor, the control system can be expressed as Fig. 3

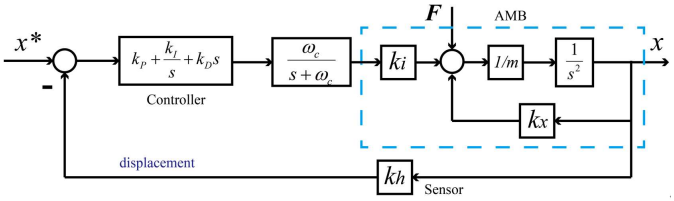

Fig. 3. Structure of control system with centrifugal force

To simplify the expression, the amplifier is regarded as a linear temporarily. Transfer function from centrifugal force to displacement is

$$\frac{X(s)}{F(s)}=\frac{G(s)/k_i}{1+k_h C(s)G(s)} \tag{5}$$

Setting $s=j\omega$, and calculating the amplitude and phase of transfer function

$$\frac{X(j\omega)}{F(j\omega)}=\frac{\omega}{j\left(k_D k_h k_i\omega^2-k_I k_h k_i\right)+\left[\left(k_P k_h k_i-k_x\right)\omega-m\omega^3\right]} \tag{6}$$

$$\left|\frac{X(j\omega)}{F(j\omega)}\right|=\frac{\omega}{\sqrt{k_h^2k_i^2\left(k_D\omega^2-k_I\right)^2+\omega^2\left(k_P k_h k_i-k_x-m\omega^2\right)^2}} \tag{7}$$

$$\angle\frac{X(j\omega)}{F(j\omega)}=\tan^{-1}\frac{k_I k_h k_i-k_D k_h k_i\omega^2}{\left(k_P k_h k_i-k_x\right)\omega-m\omega^3} \tag{8}$$

In steady state, the form of centrifugal force is $F(t)=em\omega^2\cos(\omega t+\theta_0)$. Where e is eccentricity, ω is rotating angular speed, and θ_0 is initial value of phase of centrifugal force. As a result, the amplitude of synchronous vibration in displacement is

$$X_A=em\omega^2\left|\frac{X(j\omega)}{F(j\omega)}\right|=\frac{em\omega^3}{\sqrt{k_h^2k_i^2\left(k_D\omega^2-k_I\right)^2+\omega^2\left(k_P k_h k_i-k_x-m\omega^2\right)^2}} \tag{9}$$

According to the expression of amplitude, in magnetic bearing applied PID control strategy with constant control parameters, enlarging the k_h can help reduce vibration. However, enlarging k_h also increases gain of noise, which will cause unstable system. As a result, to reduce vibration, we can enlarge sampling gain of synchronous component merely. A phase shift generalized integrator (PSGI) segment has infinite gain at its resonant frequency. So when PSGI segment is

applied in control loop of displacement, vibration in displacement can be suppressed. The GI-FLL is applied to obtain the rotating frequency from control current. However, GI-FLL is sensitive to DC component in control current, so a high-pass filter is applied before GI-FLL. The AMB control system applied vibration suppressing strategy is shown in Fig. 4.

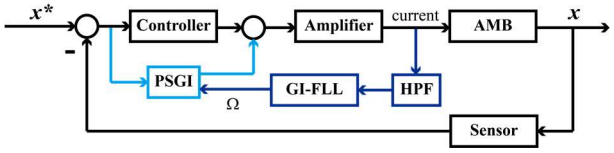

Fig. 4. Structure of AMB system applied vibration suppressing strategy

B. Anaiysis of AMB System Applied GI-FLL and PSGI

Frequency estimation segment is composed of high-pass filter (HPF) and Generalized integrator-frequency locked loop (GI-FLL). GI-FLL has been applied in power grid to estimate the frequency and shows pretty effect [12]. In AMB system, control current in coil is nearly sinusoidal with DC component. But GI-FLL is sensitivity to DC signal of input signal, DC component may cause failure of frequency estimation. As a result, a high-pass segment applied to filter out DC component is added in front of GI-FLL. The structure of frequency estimation segment is shown in Fig. 5.

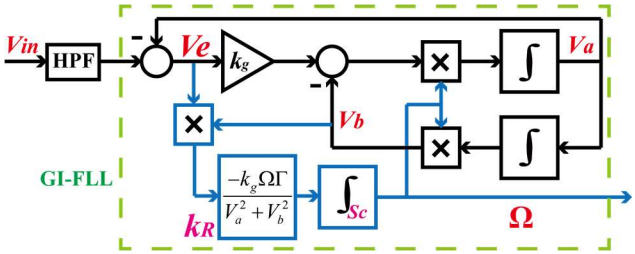

Fig. 5. Structure of frequency estimation segment

The HPF is chosen as first-order segment and its transfer function is

$$H_{F1}(s)=\frac{s}{s+\omega_H} \tag{10}$$

The transfer function of error Ve in frequency estimation segment can be expressed as

$$E(s)=\frac{V_e(s)}{V_{in}(s)}=H_{F1}(s)\frac{s^2+\Omega^2}{s^2+k_g\Omega s+\Omega^2} \tag{11}$$

$$Q(s)=\frac{V_b(s)}{V_{in}(s)}=H_{F1}(s)\frac{k_g\Omega}{s^2+k_g\Omega s+\Omega^2} \tag{12}$$

The parameter Ω is set as 200πrad/s. Drawing the bode diagrams of above transfer functions as Fig. 6. Assuming the frequency of input signal is ω=200πrad/s, if the estimated frequency Ω is larger than ω, phases of Ve and Vb are the same, product of Ve and Vb is positive, the negative gain k_R and integrator S_c will decrease Ω. If Ω is smaller than ω, phases of Ve and Vb are positive, product of Ve and Vb is negative, the negative gain k_R and integrator S_c will increase Ω. This process of adjustment stops until Ω equals to ω, which means frequency of input signal is observed. DC component of input signal causes DC component in Ve and Vb, it will destroy the adjustment process based on sign of product of Ve and Vb. There is DC component in control current, so HPF is necessary for frequency estimation by control current. Details for parameter design is introduced in paper [12].

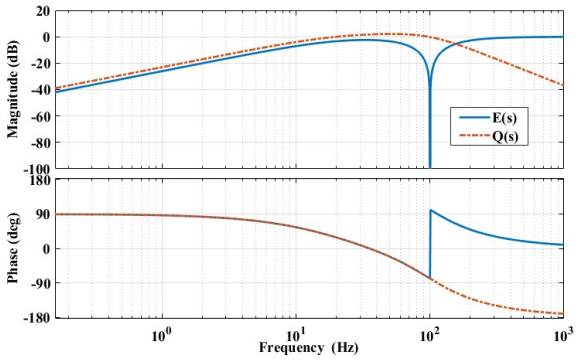

Fig. 6. Bode diagram of frequency estimation segment

To generate compensating signal, a phase shift generalized integrator (PSGI) is applied, whose structure is shown in Fig. 7.

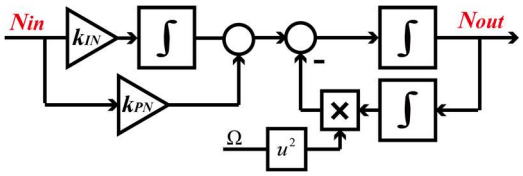

Fig. 7. Structure of PSGI

The transfer function of PSGI is

$$N(s)=\left(k_{PN}+\frac{k_{IN}}{s}\right)\frac{s}{s^2+\Omega^2} \tag{13}$$

There is infinite gain at $s=j\Omega$ of PSGI, and for common integrator 1/s, there is infinite gain at s=0. The proportional-integral (PI) segment contributes to shift phase. If the parameter are designed as $k_{PN}=\varepsilon\cos\varphi$, $k_{IN}=\varepsilon\Omega\sin\varphi$, the PI segment generates an phase phase lag φ, and gain ε when $s=j\Omega$. The resonant frequency Ω is set as 200πrad/s and ε=1, bode diagram of PSGI with various φ is shown in Fig. 8.

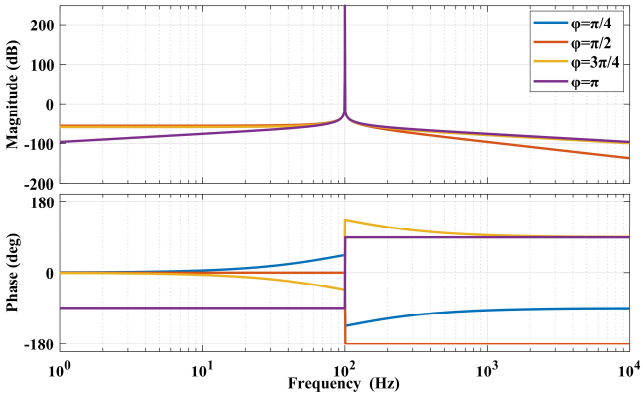

Fig. 8. Bode diagram of PSGI with various φ

The bode diagram shows that all the PSGIs have infinite gain at $s=j\Omega$ and various φ generates different phase shift at s=jΩ. When PSGI is applied to the AMB control system, the open-

loop transfer function of the control system is

$$H(s)=\left[C(s)+N(s)\right]G_1(s)G(s)k_h$$
$$=\left[\frac{k_Ps+k_I+k_Ds^2}{s}+\left(k_{PN}+\frac{k_{IN}}{s}\right)\frac{s}{s^2+\Omega^2}\right]\frac{\omega_c}{s+\omega_c}\frac{k_ik_h}{ms^2-k_x} \quad (14)$$

The characteristic equation of system is $H(s)$=-1, which can be transformed as

$$\varepsilon\frac{s\cos\varphi+\Omega\sin\varphi}{\left(s^2+\Omega^2\right)\left(\frac{k_Ps+k_I+k_Ds^2}{s}+\frac{ms^2-k_x}{k_hk_i}\frac{s+\omega_c}{\omega_c}\right)}=-1 \quad (15)$$

The root locus starts at s=±$j\Omega$ and zeros of $Z(s)$, where

$$Z(s)=\frac{k_Ps+k_I+k_Ds^2}{s}+\frac{ms^2-k_x}{k_hk_i}\frac{s+\omega_c}{\omega_c} \quad (16)$$

Because of s=±$j\Omega$ locating at virtual axis, to make the system stable, the departure angle Θ at s=±$j\Omega$ should meets $\pi/2<\Theta<3\pi/2$. The relationship between stability and departure angle Θ can be expressed as Fig. 9.

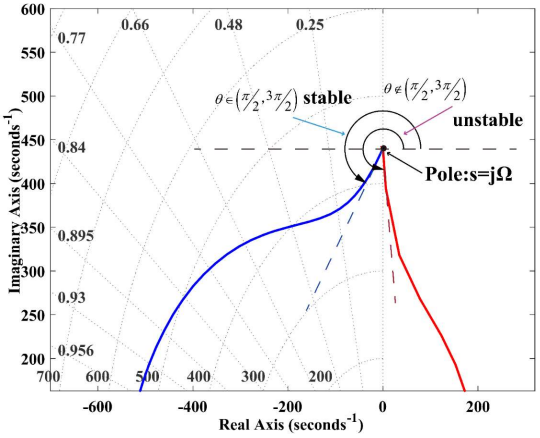

Fig. 9. Prerequisite condition of stable.

Calculating the departure angle as

$$\theta=\pi-\varphi-\arg\left(Z\left(j\Omega\right)\right) \quad (17)$$

In order to select the proper φ, the phase-frequency characteristics of $Z(s)$ is obtained as Fig. 10.

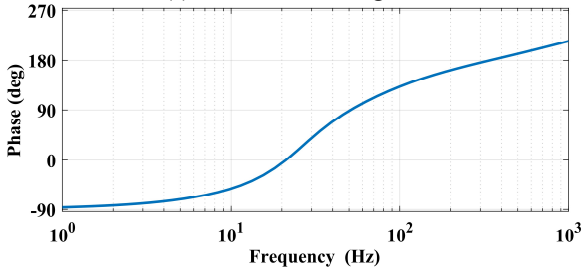

Fig. 10. Phase-frequency characteristics of $Z(s)$

To make the system stable, the parameter φ in different rotating frequency is chosen as TABLE I.

The parameter ε is designed by root locus. Drawing the root locus based on the characteristic equation as Fig. 11.

TABLE I
MAGNITUDE OF Φ IN VARIOUS ROTATING FREQUENCY

Rotating frequency	Magnitude of φ
(30Hz, 50Hz)	-45°
(50Hz, 100Hz)	-90°
(100Hz,160Hz)	-132°
>160Hz	-153°

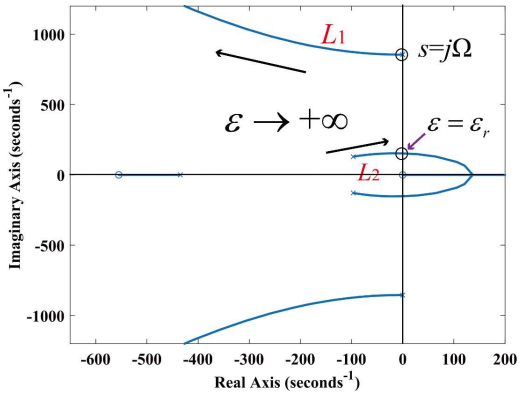

Fig. 11. Root locus of parameter ε

When ε is small, the dominant poles are mainly determined by locus L_1. Larger ε makes the root locus move farther from virtual axis, which makes the system convergent faster. Lager ε also enlarges effect of locus L_2. When ε is larger than ε_r, the root locus expand to the right of virtual axis, which means the system is unstable. In simulation or experiment, a look-up table can be made to select proper ε in various rotating speed.

When PSGI is applied in AMB system, the transfer function from centrifugal force to displacement can be derived as equation (18).

The bode diagram of this transfer function is shown in Fig.12. The rotating frequency is set as $\Omega/2\pi$=100Hz. When the frequency of excitation is 100Hz, the system performs as a notch filter. If the parameter Ω tracks rotating frequency, the displacement will not response to the centrifugal force, so vibration in displacement will be suppressed.

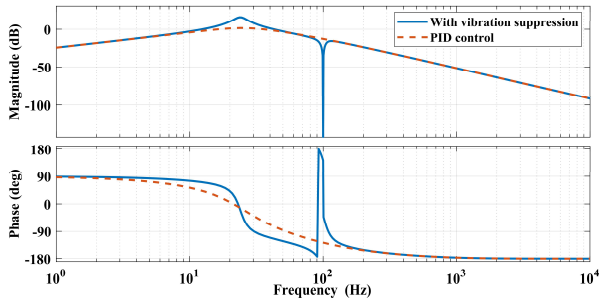

Fig. 12. Frequency response of centrifugal force in displacement.

III. SIMULATION RESULTS

Establishing the simulation model in Matlab/Simulink based on the transfer function of AMB system. The parameters are shown in TABLE II.

$$\frac{X(s)}{F(s)}=\frac{1}{\left(ms^2-k_x\right)\left(1+k_h\frac{k_i}{ms^2-k_x}\frac{\omega_c}{s+\omega_c}\left(\frac{k_Ps+k_I+k_Ds^2}{s}+\varepsilon\frac{s\cos\varphi+\Omega\sin\varphi}{s^2+\Omega^2}\right)\right)} \quad (18)$$

TABLE II
PARAMETERS OF SIMULATION

Symbol	Quantity	Magnitude
m	Mass of rotor	10kg
k_x	Stiffness	2.40×10^6N/m
k_i	Stiffness	129.7N/A
e	Eccentricity	10um
ω_c	Bandwidth of amplifier	3000π rad/s
ε	Gain of PSGI	1×10^6
k_g	Gain of GI	0.8
Γ	Gain of PLL	100

Displacement of rotor under influence of proposed vibration suppressing strategy is shown in part A, and part B presents transition process of control current and frequency estimation, which demonstrates frequency estimation is also effective when vibration reduces.

A. *Performance of Rotor while Vibration Suppressing*

The rotating speeds is set as 100Hz, at 0.3s, the high-pass filter and GI-FLL is applied to estimate the frequency by control current. At 0.8s, the PSGI is applied to reduce vibration. Fig. 13 presents results of displacement of rotor. After applying vibration suppressing strategy, the displacement of rotor is reduced significantly.

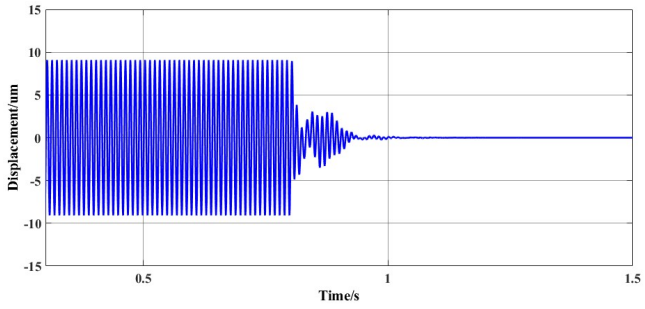

Fig. 13. Displacement of rotor when rotating frequency is 100Hz

B. *Performance of GI-FLL and Control Current while Vibration Suppressing*

When PSGI is applied to the control system, there is a transition process in both current and displacement. The GI-FLL should work efficiently in this process. Fig. 14 presents the result of control current and Fig. 15 presents the result of frequency estimation by control current. The initial value of frequency estimation is 180Hz. At 0.3s, frequency estimation is applied. At about 0.5s, there is little error between actual frequency and estimated frequency. At 0.8s, PSGI is applied, there is a transition process in control current, the GI-FLL can also estimate the rotating frequency.

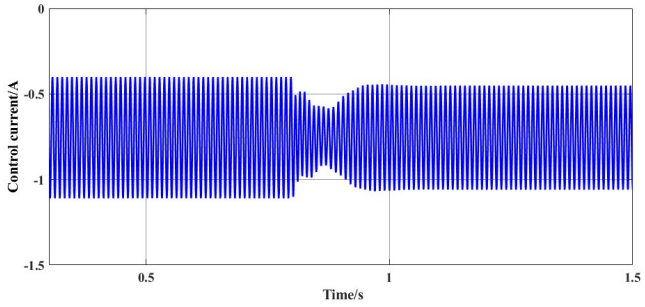

Fig. 14. Perforamce of control current when PSGI is applied

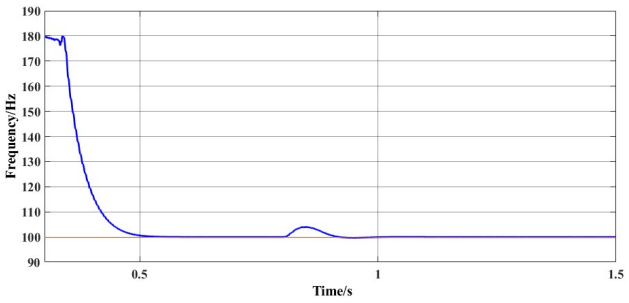

Fig. 15. Frequency estimation when PSGI is applied

IV. EXPERIMENTAL RESULTS

To verify the effectiveness of the vibration suppressing strategy, experiments have been carried out on an AMB test rig. There are four degrees of freedom in radial controlled by two radial AMB. The shaft is driven by a high-speed motor. Two touchdown bearings are applied to protect the AMBs. Fig. 16 shows the components and arrangement of the test rig.

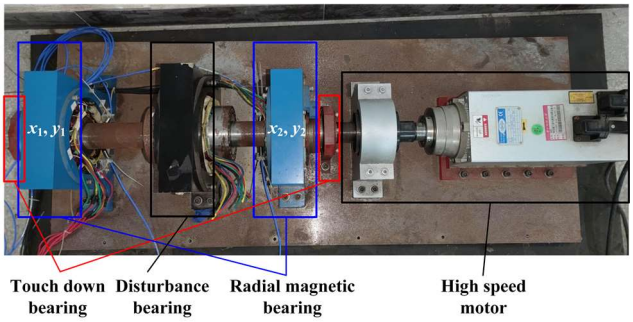

Fig. 16. Structure of magnetic bearing test rig

The structure of amplifier is shown in Fig. 17, the control board receives displacement with current signal and generate PWM signal by control algorithm. The switching device is IGBT and the switching frequency is set as 20kHz. The DC bus voltage is 150V and the bias current of AMB is 5A.

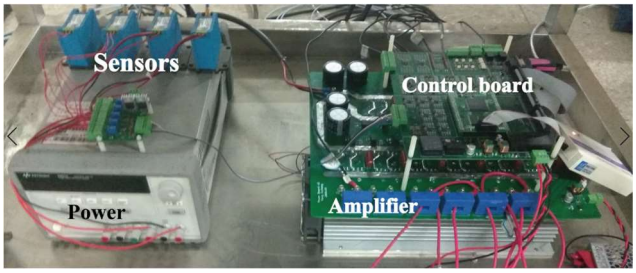

Fig. 17. Structure of amplifier and controller

Parameters used in experiment is shown in TABLE III. Because of modeling error, parameters of PSGI is different from simulation. Other parameters are same as TABLE II.

TABLE III
PARAMETERS OF EXPERIMENTS

Symbol	Quantity	Magnitude
ε	Gain of PSGI	1×10^5
φ	Phase shift	-135°
k_P	Proportion	2.64×10^4
k_I	Integration	5×10^5
k_D	Differentiation	48

A. Displacement of Rotor while Vibration Suppressing at Constant Rotating Frequency

The displacement of rotor is shown in Fig. 18 and whose spectrum is shown in Fig. 19. The rotating speed is set as 80Hz, before the vibration suppressing strategy is applied, the amplitude of synchronous vibration is about 80.49μm. After applying suppressing strategy, the synchronous vibration reduces to 2.06μm, which shows the effectiveness of the suppressing strategy.

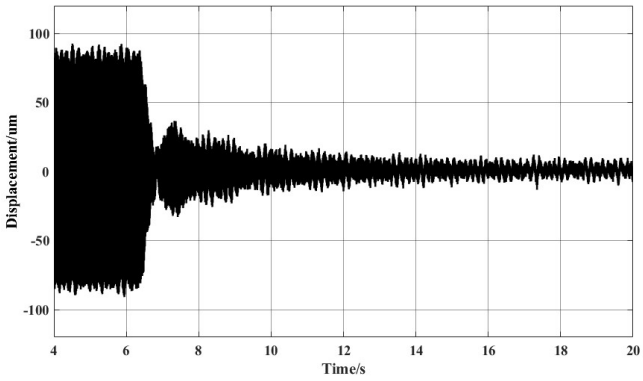

Fig. 18. Displacement of rotor without and with proposed strategy

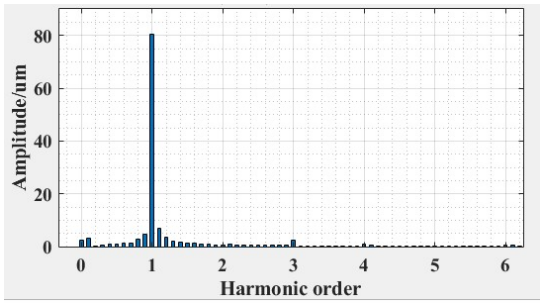

(a)Spectrums of displacement without proposed strategy

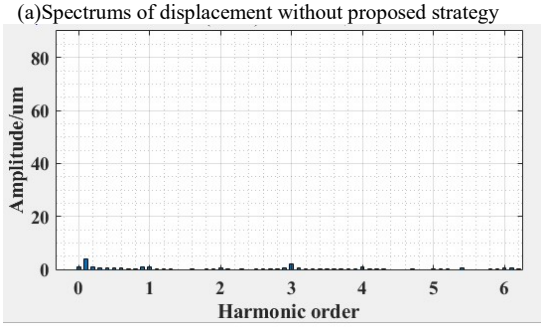

(b)Spectrums of displacement with proposed strategy

Fig. 19. Spectrums of displacement

B. Performance of GI-FLL and Control Current while Vibration Suppressing at Constant Rotating Frequency

Transition process of control current is shown in Fig. 20. The DC component in control current is about 3A. Result of frequency estimation is shown in Fig. 21. The error between actual frequency and estimated frequency is about ±0.5Hz before PSGI is applied. After applying PSGI, the frequency error increases to about ±2Hz, but this error hardly influences effect of vibration suppressing. This error is mainly caused by two factors: firstly, there is noise in current signal. Then, when PSGI is applied, synchronous vibration of control current is also reduced, the frequency estimation mainly utilizes the synchronous vibration in control current, so result of frequency estimation is also affected by harmonic vibration.

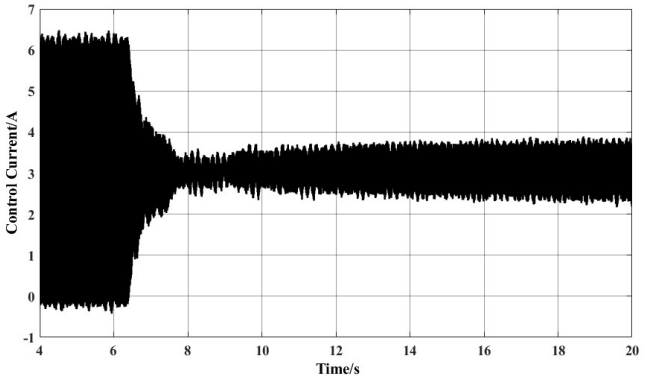

Fig. 20. Performance of control current when PSGI is applied

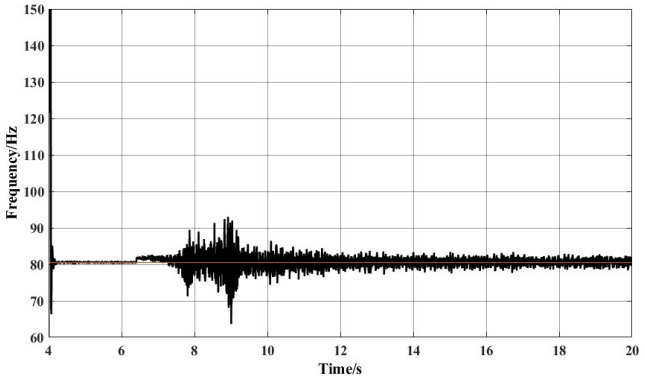

Fig. 21. Frequency Estimation when PSGI is applied

C. Performance of Rotor while Vibration Suppressing at Variable Rotating Frequency

Accelerating rotating frequency from 50Hz to 70Hz. Result of displacement is shown in Fig. 22. In 0-12s, the rotor rotates with proposed vibration suppression strategy, the amplitude of vibration is about ±5μm. In 12-22s, rotating frequency accelerates from 50-70Hz, and during acceleration, GI-FLL and PSGI are applied at the same time. At 40s, displacement reduces to ±5μm. When the rotor rotates at 50Hz and 70Hz without vibration suppression, the amplitude of vibration is larger than 50μm. This result presents that after transition process caused by acceleration, the proposed strategy also works effectively. However, the frequency estimation should be improved to adopt accelerating.

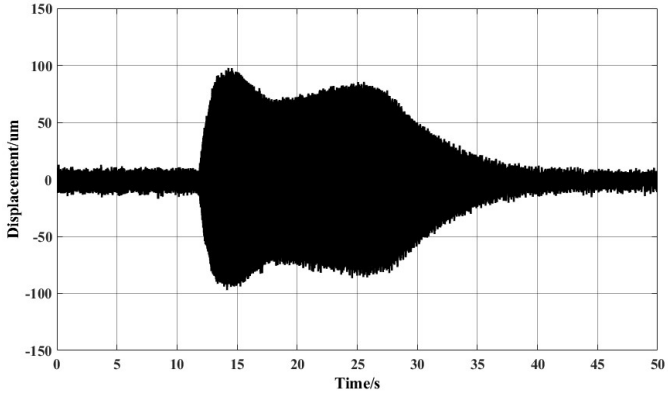

Fig. 22. Displacement while accelerating

Transition process of control current while accelerating is shown in Fig. 23. Results of frequency estimation is shown in Fig. 24. The vibration in current while accelerating increases but reduces after acceleration. The result of frequency estimation shows that GI-FLL can estimate the rotating frequency while accelerating to support the PSGI for vibration suppression.

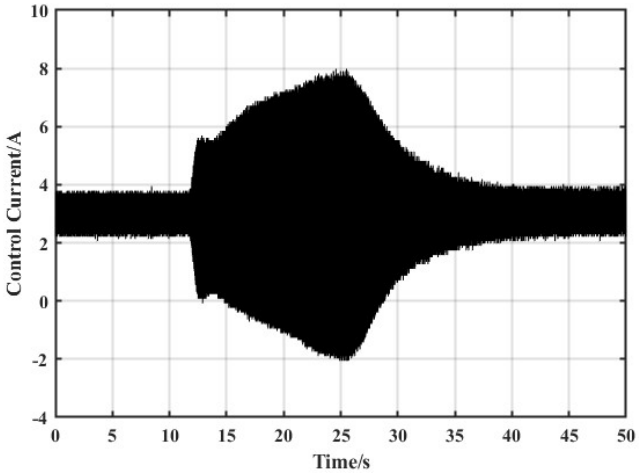

Fig. 23. Performance of control current while accelerating

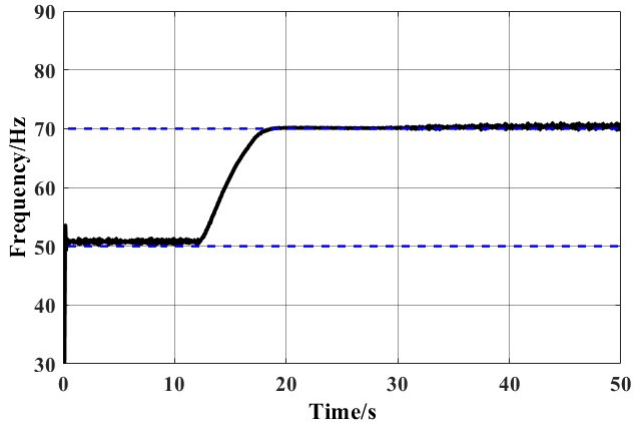

Fig. 24. Frequency estimation while accelerating

V. CONCLUSIONS

This paper analyzed performance of rotor by influenced of centrifugal force in AMB system. The amplitude and phase of synchronous vibration in displacement is calculated in theory. Considering that angular speed sensor is necessary in most of vibration reduction methods, this paper proposed a vibration suppressing strategy without angular speed sensor based on GI-FLL and PSGI. GI-FLL is applied to obtain rotating speed by control current and HPF is used to filter out DC component in control current. PSGI generates compensating signal to suppress vibration. The value of compensating phase φ and the effect of parameter ε is analyzed by root locus. Results of simulations and experiments demonstrate the effectiveness of vibration reduction effect of proposed vibration suppressing strategy in constant rotating speed. The robustness for frequency estimating while speed changing will be further improved. Then, the stability analysis of proposed control strategy is carried out for the single degree of freedom system in this paper. However, the four degrees of freedom of radial motion are coupled in AMB-rotor systems. Thorough analysis of stability considering coupling effect and nonlinear effect will be further researched.

REFERENCES

[1] Schweitzer G, Maslen E H. *Magnetic bearings: theory, design, and application to rotating machinery*[*M*]// Magnetic Bearings—Theory, Design and Application to Rotating Machinery. 2009.

[2] S. Zheng, B. Han, R. Feng and Y. Jiang, "Vibration Suppression Control for AMB-Supported Motor Driveline System Using Synchronous Rotating Frame Transfermation," *IEEE Transactions on Industrial Electronics*, vol. 62, no. 9, pp. 5700-5708, Sept. 2015.

[3] R. Herzog, P. Buhler, C. Gahler and R. Larsonneur, "Unbalance compensation using generalized notch filters in the multivariable feedback of magnetic bearings," *IEEE Transactions on Control Systems Technology*, vol. 4, no. 5, pp. 580-586, Sept. 1996.

[4] P. Cui, S. Li, Q. Wang, Q. Gao, J. Cui and H. Zhang, "Harmonic Current Suppression of an AMB Rotor System at Variable Rotation Speed Based on Multiple Phase-Shift Notch Filters," *IEEE Transactions on Industrial Electronics*, vol. 63, no. 11, pp. 6962-6969, Nov. 2016.

[5] C. Peng, S. Zheng, Z. Huang and X. Zhou, "Complete Synchronous Vibration Suppression for a Variable-Speed Magnetically Suspended Flywheel Using Phase Lead Compensation," *IEEE Transactions on Industrial Electronics*, vol. 65, no. 7, pp. 5837-5846, July 2018.

[6] Jiang K, Zhu C, Chen L. "Unbalance Compensation by Recursive Seeking Unbalance Mass Position in Active Magnetic Bearing-Rotor System". *IEEE Transactions on Industrial Electronics*, vol. 62, no. 9, pp. 5655-5664, 2015.

[7] Mao C, Zhu C. "Unbalance Compensation for Active Magnetic Bearing Rotor System Using a Variable Step Size Real-Time Iterative Seeking Algorithm". *IEEE Transactions on Industrial Electronics*, vol. 65, no. 5, pp. 4177-4186, 2018.

[8] H. Sun, D. Jiang, Z. Hu, T. Li and J. Lai, "Unbalance Vibration Compensation of Magnetic Bearing Systems based on Beetle Antennae Search Algorithm," in *Proc. of* 2019 *IEEE International Electric Machines & Drives Conference* (*IEMDC*), San Diego, CA, USA, 2019, pp. 1937-1943.

[9] Bi C , Wu D , Jiang Q , et al. "Automatic learning control for unbalance compensation in active magnetic bearings". *IEEE Transactions on Magnetics*, vol. 41, no. 7, pp. 2270-2280, 2005.

[10] W. Lee, S. S. Oh and D. Cheong, "Rotor unbalance compensation without angular position sensor for Active Magnetic Bearing," in *Proc. of* 8*th International Conference on Power Electronics - ECCE Asia*, Jeju, 2011, pp. 2446-2449.

[11] Q. Chen, G. Liu and B. Han, "Suppression of Imbalance Vibration in AMB-Rotor Systems Using Adaptive Frequency Estimator," *IEEE Transactions on Industrial Electronics*, vol. 62, no. 12, pp. 7696-7705, Dec. 2015.

[12] P. Rodríguez, A. Luna, I. Candela, R. Mujal, R. Teodorescu and F. Blaabjerg, "Multiresonant Frequency-Locked Loop for Grid Synchronization of Power Converters Under Distorted Grid Conditions," *IEEE Transactions on Industrial Electronics*, vol. 58, no. 1, pp. 127-138, Jan. 2011.

[13] Shafai B, Beale S, Larocca P, et al. "Magnetic bearing control systems and adaptive forced balancing". *Control Systems IEEE*, vol. 14, no. 2, pp. 4-13, 1994.

[14] Hutterer M, Schrcödl M. Unbalance compensation of a magnetically levitated rotor for the whole operating range", in *Proc. of IEEE International Conference on Mechatronics*. IEEE, 2017, pp. 226-231.

[15] Z. Hu, D. Jiang, H. Sun and R. Qu, "A Shared-bridge Converter with Reversed Current Direction for Active Magnetic Bearing Drive," in *Proc. of* 2019 10*th International Conference on Power Electronics and ECCE Asia* (*ICPE 2019 - ECCE Asia*), Busan, Korea (South), 2019, pp. 1-7.

[16] Xu X, Liu J, Chen S. "Synchronous Force Elimination in the Magnetically Suspended Rotor System With an Adaptation to Parameter Variations in the Amplifier Model". *IEEE Transactions on Industrial Electronics*, vol. 65, no. 12, pp. 9834 – 9842, 2018.

[17] Yoon S Y , Di L , Lin Z . “Unbalance compensation for AMB systems with input delay: An output regulation approach”. *Control Engineering Practice*, vol. 46, 166-175, 2016.

[18] Hutterer M , Kalteis G , Schrodl M . “Redundant unbalance compensation of an active magnetic bearing system”. *Mechanical Systems and Signal Processing*, vol. 94, pp. 267-278, 2017.

[19] Jiang D, Kshirsagar P. “Analysis and Control of a Novel Power Electronics Converter for Active Magnetic Bearing Drive”. *IEEE Transactions on Industry Applications*, vol. 53, no. 3, pp. 1-1, 2017.

[20] Jiang D , Li T , Hu Z , et al. “Novel Topologies of Power Electronics Converter as Active Magnetic Bearing Drive”. *IEEE Transactions on Industrial Electronics*, vol. 67, no.2, pp. 950 – 959, 2020.

[21] Z. Xin, R. Zhao, P. Mattavelli, P. C. Loh and F. Blaabjerg, "Re-Investigation of Generalized Integrator Based Filters From a First-Order-System Perspective," *IEEE Access*, vol. 4, pp. 7131-7144, 2016.

[22] Wu Y , Ren G P , Zhang H T . “Dual-mode predictive control of a rotor suspension system”. *ence China Information ences*, vol. 63, no.1, 2020.

[23] Yongchang Zhang, Lanlan Huang, Donglin Xu, Jiali Liu, Jialin Jin. “Performance Evaluation of Two-Vector-Based Model Predictive Current Control of PMSM Drives”. *Chinese Journal of Electrical Engineering*, vol. 4, no. 2, pp. 65-81, 2018.

[24] Jikai Si, Suzhen Zhao, Lufeng Zhang, Ruiwu Cao, Wenping Cao. “The Characteristics Analysis and Cogging Torque Optimization of a Surface-Interior Permanent Magnet Synchronous Motor”. *Chinese Journal of Electrical Engineering*, vol. 4, no. 4, pp. 41-47, 2018.

Hongbo Sun (S’19) was born in Shandong, China, in 1995. He received the B.S. degree in hydraulic engineering, from Huazhong University of Science &Technology, Wuhan, China, in 2018. He is currently working toward the M.S. degree in the School of Electronic and Electrical Engineering, Huazhong University of Science &Technology, Wuhan, China.
His current research focuses on vibration suppression of active magnetic bearing.

Dong Jiang (S05’-M12’-SM16’) received B.S and M. S degrees in electrical engineering from Tsinghua University, Beijing, China, in 2005 and 2007 respectively. He began his Ph.D. study in Center for Power Electronics Systems (CPES) in Virginia Tech in 2007 and was transferred to University of Tennessee with his advisor in 2010. He received his Ph.D. degree in power electronics and motor drives from University of Tennessee in Dec. 2011. He was with United Technologies Research Center (UTRC) in Connecticut as a Senior Research Scientist/Engineer from Jan 2012 to July 2015. He has been with Huazhong University of Science &Technology (HUST) in China as a professor since July 2015. Dong Jiang’s major research area is power electronics and motor drives, with more than 100 published IEEE journal and conference papers in this area. He has four best paper awards in IEEE conferences. He is an associate editor of IEEE Transactions on Industry Applications.

Jichang Yang was born in Hunan, China, in 1997. He received the B.S. degree in electrical engineering, from Huazhong University of Science &Technology, Wuhan, China, in 2019. He is currently working toward the M.S. degree in the School of Electronic and Electrical Engineering, Huazhong University of Science &Technology, Wuhan, China.
His current research focuses on novel converter topology of active magnetic bearing.